2.4/5.7-GHz CMOS Dual-Band Low-IF Architecture Using Weaver–Hartley Image-Rejection Techniques

Chin-Chun Meng, *Member, IEEE*, Tzung-Han Wu, *Member, IEEE*, Jin-Siang Syu, Sheng-Wen Yu, Kuan-Chang Tsung, and Ya-Hui Teng

***Abstract*—A 2.4/5.7-GHz dual-band Weaver–Hartley architecture, using 0.18-μm CMOS technology, is demonstrated in this paper. The 2.4-GHz signal is set to be the image signal when the desired signal is at 5.7 GHz, and vice versa. Since the Weaver and Hartley systems are combined into this architecture, the demonstrated architecture rejects not only the first image signal, but also the secondary image signal. The image-rejection ratios of the first image signal and the secondary image signal are better than 40 and 46 dB, respectively. In this paper, a diagrammatic explanation is employed to obtain the image-rejection mechanisms of the Weaver–Hartley architecture.**

***Index Terms*—Divider, Hartley architecture, image rejection, secondary image rejection, Weaver architecture.**

I. Introduction

THE PROBLEM of image signal exists in all of the wireless communication systems. In the past, an off-chip image-rejection filter has been employed to reject the image signal; however, the off-chip components limit the circuit integration, and thus, need to be removed. As a result, many highly integrated image-rejection architectures have been developed. One of the most popular image-rejection systems is the direct-conversion system. The direct-conversion architecture [1] eliminates the image signal by setting the IF frequency at zero instead of using the image-rejection filters. Although the integration level of the direct-conversion system can be very high, this system suffers from two serious issues: the dc offset caused by the signal self-mixing problem [1] and the mixer low-frequency noise resulting from the transistor $1/f$ noise [2]. Sub-harmonic mixers and area-consuming on-chip dc blocking capacitors are employed to prevent the dc offset problem and the transistor $1/f$ noise. Sometimes much more complicated octet-phase local oscillator (LO) generation circuits are required for the direct-conversion system [3], [4]. Moreover, extra circuit techniques are necessary to improve the low-frequency noise figure (NF) of a CMOS direct-conversion mixer [5]–[7]. On the other hand, the low-IF system is useful to reject the image signal, and thus, the issues in the direct-conversion mixer are absent. The Hartley low-IF architecture is capable of rejecting image signals using the complex polyphase filters [8]–[12]. Since the IF frequency is not zero, the dc offset and the transistor $1/f$ noise can be distinguished from the signal.

Another useful image-rejection system is the Weaver system [13]–[18]. The Weaver system is a dual-conversion system, but does not require a filter when compared with the heterodyne system. The integration level of the Weaver architecture is also high because no off-chip image-rejection filter is required. The Weaver system can effectively eliminate the first image signal, but the Weaver structure suffers from the secondary image problem if the final IF is not set at zero [16]. A single-band low-IF dual-conversion system is implemented in [10] and [17], and the secondary image is rejected by the polyphase filter in the second IF stage [10], while the first image is removed by the dual conversion mechanism [14], [18].

Most of the multiband RF transceivers are implemented using direct-conversion architectures [19]–[22]. These multiband receivers use multiple local area networks (LNAs) and mixers to deal with each particular RF band. The direct-conversion system also requires extra approaches to eliminate the $1/f$ noise in the mixer stage [5]–[7]. In addition, the mixers cannot be reused for most of the transceivers [19]–[21]. Some dual-band dual-conversion Weaver systems are demonstrated and the secondary image problem is avoided because the final IF in the second stage is set at zero [16]. Thus, this receiver still suffers from the $1/f$ noise and dc offset problem; in addition, the mixers are not reused [16]. Moreover, most of these zero-IF multiband receivers require more than one LO [19], [21], [22]. Since the IF frequency is zero in the direct-conversion system, it is very difficult to design a voltage-controlled oscillator (VCO) covering the 2.4- and 5.7-GHz bands by using simple dividing or multiplying. The extra VCO can cause substrate crosstalk and spurious signals.

In this paper, a 2.4/5.7-GHz dual-band low-IF down-converter system that combines both Weaver and Hartley architectures [9], [14] is demonstrated using the 0.18-μm CMOS technology. The main application of this study is the wireless LAN 802.11 a/g. The architecture used here combines the advantages reported in previous literatures, and thus, a dual-band system without the secondary image problem is achieved. When the desired signal is at 5.7 GHz, the 2.4-GHz band is set at the image signal of the Weaver structure and vice versa [16],

Manuscript received July 01, 2008; revised November 01, 2008. First published February 03, 2009; current version published March 11, 2009. This work was supported by the National Science Council of Taiwan under Contract NSC 95-2221-E-009-043-MY3 and Contract NSC 97-2221-E-009-171, by the Ministry of Economic Affairs of Taiwan under Contract 96-EC-17-A-05-S1-020, and by the Ministry of Education (MoE) ATU Program under Contract 95W803.

C.-C. Meng, J.-S. Syu, S.-W. Yu, K.-C. Tsung, and Y.-H. Teng are with the Department of Communication Engineering, National Chiao Tung University, Hsinchu 300, Taiwan (e-mail: ccmeng@mail.nctu.edu.tw; jssyu.cm95g@nctu.edu.tw; awn.cm93g@nctu.edu.tw; slashrose.cm94g@nctu.edu.tw; fifiya.cm95g@nctu.edu.tw).

T.-H. Wu was with the Department of Communication Engineering, National Chiao Tung University, Hsinchu 300, Taiwan. He is now with MediaTek, Hsinchu 300, Taiwan (e-mail: amoswu.cm92g@nctu.edu.tw).

Color versions of one or more of the figures in this paper are available online at http://ieeexplore.ieee.org.

Digital Object Identifier 10.1109/TMTT.2008.2012300

[23]. The LO_1 frequency is chosen to be 4.05 GHz, which is halfway between 2.4–5.7 GHz. The 2.4/5.7-GHz band selection is achieved by changing the polarization of the complex LO_1 (the first LO) signals. Since a low-IF architecture is employed in this study, it is very easy to perform a frequency arrangement that only needs one on-chip VCO. An LO generator consisting of a new 50% duty cycle divide-by-five circuit and a truly balanced multiplier is employed to generate the 1.62-GHz LO_2 (the second LO) signal for the Weaver system and to increase the image-rejection performance of the entire system [18]. Thus, the IF frequency of this low-IF down-converter is around 30-MHz. As a result, the extra VCO is not needed, and its complexity is reduced. Compared with previous literatures, the demonstrated Weaver–Hartley system has the competitive rejection performance of the first image and secondary image signals [14]–[18] because of the double-quadrature Hartley system [9], [12] and the coherence between the LO_1 and LO_2 signals [18]. Besides, the mixer stages can be reused in our Weaver–Hartley structure.

The operational principle and frequency planning of the proposed Weaver–Hartley image-rejection architecture are discussed in Section II. The diagrammatic complex mixing explanation [12], [18], [23] is employed to illustrate the image-rejection mechanisms of this hybrid Weaver–Hartley architecture. Section III describes the circuit implementation in detail, and Section IV reports the measurement results.

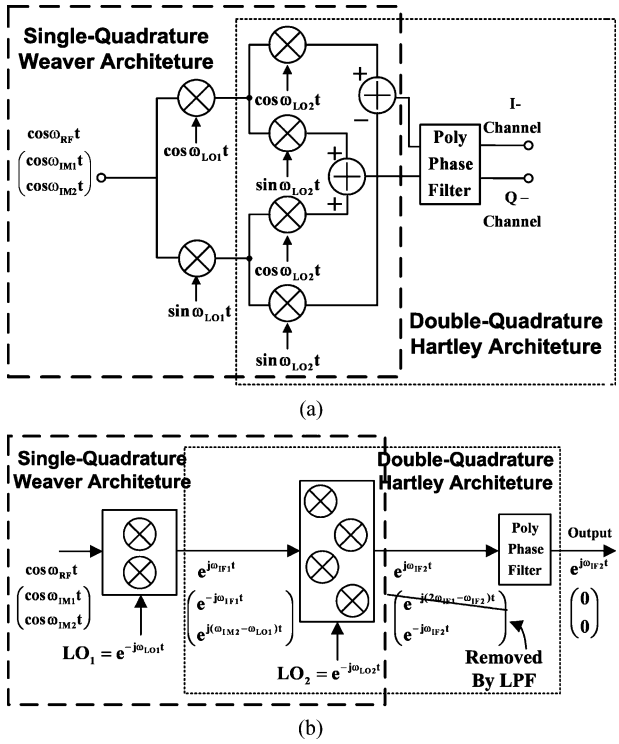

Fig. 1. (a) Block diagram of the Weaver–Hartley architecture. (b) Complex signal representation of the Weaver–Hartley architecture.

II. Weaver–Hartley Image-Rejection Architecture

The block diagram of the proposed Weaver–Hartley image-rejection structure is shown in Fig. 1(a). The angular frequencies of the desired, first image and secondary image signals are denoted as ω_{RF}, ω_{IM1} and ω_{IM2}, respectively. The angular frequencies of the LO_1 and LO_2 signals are denoted as ω_{LO1} and ω_{LO2}. The frequency of the IF signal down-converted by the first-stage mixers is defined as ω_{IF1}, while the frequency of the IF signal down-converted by the second-stage mixers is defined as ω_{IF2}. The relationship between the above signals is given in the following:

$$\begin{aligned}\omega_{\mathrm{IF1}} &= \omega_{\mathrm{RF}} - \omega_{\mathrm{LO1}} \\ &= \omega_{\mathrm{LO1}} - \omega_{\mathrm{IM1}} \qquad (1a)\\ \omega_{\mathrm{IF2}} &= \omega_{\mathrm{RF}} - (\omega_{\mathrm{LO1}} + \omega_{\mathrm{LO2}}) \\ &= \omega_{\mathrm{LO1}} + \omega_{\mathrm{LO2}} - \omega_{\mathrm{IM2}} \\ &= \omega_{\mathrm{IF1}} - \omega_{\mathrm{LO2}}. \qquad (1b)\end{aligned}$$

As shown in Fig. 1(a), the first half of the down-converter is a single-quadrature Weaver system including six multipliers [14], [18]. The other half of the down-converter is a double-quadrature Hartley system consisting of four multipliers and a four-section polyphase filter [9]. The Weaver–Hartley image-rejection system is formed by sharing four mixers, as shown in Fig. 1(a). When the frequency of the desired signal is 5.7 GHz (2.4 GHz), and the LO_1 frequency is 4.05 GHz, the dual-conversion Weaver system then perfectly rejects the first image signal whose frequency is close to 2.4 GHz (5.7 GHz), and the frequency of the secondary image signal is around 5.64 GHz (2.46 GHz). In order to explain the function of the Weaver–Hartley structure, the complex signal-block diagram representation for complex mixers is shown in Fig. 1(b).

A. Rejection of the First Image Signal

Instead of the conventional trigonometric analysis, the complex-signal diagrammatic explanation shown in Fig. 2 gives a direct insight to the RF system architecture. The RF signal and quadrature LO signals can be denoted as $\cos\omega_{\mathrm{RF}}t$ and $e^{-j\omega_{\mathrm{LO}}t}$, respectively. On the other hand, the first image signal and secondary image signal can be expressed as $\cos\omega_{\mathrm{IM1}}t$ and $\cos\omega_{\mathrm{IM2}}t$, respectively. Fig. 2(a) shows the corresponding spectra of the ω_{RF}, ω_{IM1}, and ω_{IM2} signals.

Since the quadrature LO_1 signal $(e^{-j\omega_{\mathrm{LO1}}t})$ is located at the negative spectrum, the RF signal shifts to the left after down-conversion mixing [12], [18], [23]. In other words, after the complex LO_1 down-conversion, the positive RF complex frequency shifts to the positive ω_{IF1} complex frequency and the negative RF complex frequency shifts to the negative frequency of $(\omega_{\mathrm{LO1}}+\omega_{\mathrm{RF1}})$, as shown in Fig. 2(b). Thus, the negative frequency spectrum in Fig. 2(b) can be omitted in the analysis for the sake of simplicity.

Next, the signals in Fig. 2(b) are down-converted further by the subsequent second-stage complex mixer. Similarly, the quadrature $\mathrm{LO}_2(\mathrm{e}^{-j\omega_{\mathrm{LO2}}t})$ signal of the second-stage complex mixer is located at the negative spectrum. Therefore, the signals in Fig. 2(b) shift to the left in the spectrum again, as shown in Fig. 2(c). This process can be expressed by the complex signal

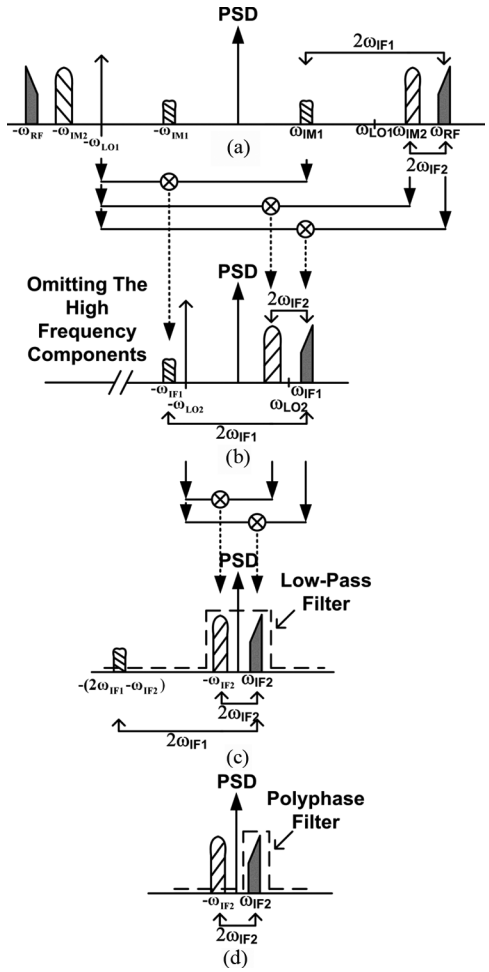

Fig. 2. (a) RF, IM_1, and IM_2 signal spectra. (b) Signals after down-converting by the first stage complex mixer. (c) Signals after down-converting by the second stage complex mixer. (d) Signals filtered by the final IF polyphase filters.

multiplication [12], [18], [23] as

$$\cos\omega_{\mathrm{RF}}t \times \mathrm{e}^{-j\omega_{\mathrm{LO1}}t} \times \mathrm{e}^{-j\omega_{\mathrm{LO2}}t} = \frac{\mathrm{e}^{j\omega_{\mathrm{IF2}}t} + \mathrm{e}^{-j(\omega_{\mathrm{RF}}+\omega_{\mathrm{LO1}}+\omega_{\mathrm{LO2}})t}}{2}. \quad (2a)$$

Similarly, the shifted IM_1 and IM_2 signals can be represented as

$$\cos\omega_{\mathrm{IM1}}t \times \mathrm{e}^{-j\omega_{LO1}t} \times \mathrm{e}^{-j\omega_{\mathrm{LO2}}t} = \frac{\mathrm{e}^{-j(2\omega_{\mathrm{IF1}}-\omega_{\mathrm{IF2}})t} + \mathrm{e}^{-j(\omega_{\mathrm{IM1}}+\omega_{\mathrm{LO1}}+\omega_{\mathrm{LO2}})t}}{2} \quad (2b)$$

$$\cos\omega_{\mathrm{IM2}}t \times \mathrm{e}^{-j\omega_{\mathrm{LO1}}t} \times \mathrm{e}^{-j\omega_{\mathrm{LO2}}t} = \frac{\mathrm{e}^{-j\omega_{\mathrm{IF2}}t} + \mathrm{e}^{-j(\omega_{\mathrm{IM2}}+\omega_{\mathrm{LO1}}+\omega_{\mathrm{LO2}})t}}{2}. \quad (2c)$$

The RF signal is down-converted to the positive ω_{IF2} complex frequency, as shown in Fig. 2(c). On the other hand, the first image signal ω_{IM1} is down-converted to the negative $(2\omega_{\mathrm{IF1}} - \omega_{\mathrm{IF2}})$ complex frequency. Due to the dual conversion phenomena, the first image signal can be easily filtered out by the low-pass filter, as shown in Fig. 2(c). Normally, the frequency response of the IF circuits can serve as the low-pass filter as long as ω_{IF1} is large enough.

B. Rejection of the Secondary Image Signal

The dual-conversion down-converter still suffers from the secondary image signal problem [16], and the frequency of the secondary image signal is $2\omega_{\mathrm{IF2}}$ away from the RF frequency, as shown in Fig. 2(c). The secondary image signal is also shifted downward twice by the two complex mixers of the Weaver system. However, the down-converted secondary image signal is not shifted outside the frequency response of the low-pass filter as with the first image signal IM_1. Instead, the frequency of the down-converted secondary image signal is shifted to the negative ω_{IF2} spectrum, while the down-converted RF signal is located at ω_{IF2}, as shown in Fig. 2(c). This down-converted secondary image signal cannot be filtered out by the low-pass filter and disturbs the down-converted desired RF signal. On the other hand, the polyphase filter [9], [11], which is an asymmetrical complex notch filter, can filter out the down-converted secondary image signal by eliminating the signals in the negative spectrum, as illustrated in Fig. 2(d).

It is worthwhile to mention that the second-stage complex mixer and the IF polyphase filter form a double-quadrature Hartley system [9]. The second-order error inherent in the double-quadrature system is less than the first-order error in the single-quadrature system. The double-quadrature Hartley system has better immunity to signal mismatches and is thus chosen for the second-stage mixer in this study. As a result, the demonstrated dual-band Weaver–Hartley system has more immunity to the nonideal effects caused by signal mismatches for the secondary image rejection.

The double-quadrature multiplier can also certainly be employed as the first-stage mixer of the Weaver–Hartley system because a double-quadrature multiplier tolerates more signal mismatches than a single-quadrature multiplier does. However, the higher first-image-rejection ratio is achieved at the cost of a higher NF because a polyphase filter is employed to obtain the quadrature RF signals [9]. The other reason for using a single-quadrature Weaver system instead of a double-quadrature Weaver architecture, as shown in Fig. 1, is to reduce complexity. The band selection function is more complicated and requires switches in both of the RF and LO paths. Thus, the first stage of this dual-band Weaver–Hartley down-converter is chosen to be a single-quadrature Weaver system.

Moreover, there is another advantage in such a dual conversion image-rejection system. Since the frequency of the first image signal is far away from that of the desired RF signal, all of the building blocks within the receiver chain, such as the antenna, filters, and LNA can attenuate the first image signal to some degree. Obviously, two separate narrowband LNAs can be connected to this dual-band Weaver–Hartley architecture to provide extra image rejection by attenuating the first image signals if IF_1 is properly chosen [17]. However, either a concurrent dual-band LNA [24], switch-band LNA, or wideband LNA is also adequate to connect this receiver because the proposed topology guarantees the basic image-rejection ratio.

C. Spurious Response, Frequency Planning, and Band Selection

The desired signals are around 5.7 and 2.4 GHz, respectively; therefore, the LO_1 signal for the Weaver system is set to be 4.05 GHz. In order to achieve the resulting IF_2 bandwidth within several tens of megahertz, a divide-by-2.5 divider for generating the LO_2 signal of 1.62 GHz from the LO_1 signal is designed in our frequency planning. Coherent LO_1 and LO_2 signals are useful to maximize the image-rejection ratio [18].

The down-converted spurs have the frequencies of $(kf_{\mathrm{RF}} \pm mf_{\mathrm{LO1}} \pm nf_{\mathrm{LO2}})$ [16]. If the LO_1 frequency is the integer multiple of the LO_2 frequency, the spurious response can easily fall into the final IF channels and degrade the performance of the image-rejection receiver. On the other hand, the spurious components can hardly fall into the IF channels if the LO_1 frequency is the fractional multiples of the LO_2 frequency.

In this study, the divide-by-five circuit and frequency doubler are employed to provide a divide-by-2.5 divider. The spreadsheet enumerating method is employed to calculate the mixing terms of the RF, LO_1, and LO_2 signals with their fundamental, second, third, fourth, and fifth harmonics. There is no interfering signal caused by the spurious tone down-converted into the IF bandwidth, except for one mixing combination. The only down-converted spur is $(f_{\mathrm{RF}} - 3f_{\mathrm{LO1}} + 4f_{\mathrm{LO2}})$. However, the spurious signal is very small because the even harmonics are greatly suppressed in the double-balanced system.

There are two sources for the spurious signals. One is the spurious down-conversion of the desired RF signals as discussed. The other is spurious response to the undesired signals because the sliding-IF dual-conversion architecture receives a wide variety of signals [21]. The undesired RF frequency is equal to $mf_{\mathrm{LO1}} + nf_{\mathrm{LO2}} \pm f_{\mathrm{IF2}}$ and only odd numbers of m and n are considered because the double-balanced Gilbert mixer is employed. Thus, an exhausted search for $m, n \in \{\pm 1, \pm 3, \pm 5\}$ is performed and the resulting spurious undesired RF signals below 10 GHz are discussed in this paper. As a consequence, except for the desired RF and image signals (either 2.4 or 5.7 GHz) with LO indices $(m, n) = (1, \pm 1)$, there are still five undesired RF signals with LO indices $(m, n) = (1, 3)$, $(3, -3)$, $(-1, 3)$, $(3, -5)$, and $(-1, 5)$ corresponding to $8.91 \pm f_{IF2}$, $7.29 \pm f_{\mathrm{IF2}}$, $0.81 \pm f_{\mathrm{IF2}}$, $4.05 \pm f_{\mathrm{IF2}}$, and $4.05 \pm f_{\mathrm{IF2}}$ GHz, respectively. Thus, a preceding LNA (or filter) with either a dual- or switched-band topology is preferable for practical use [24]. A properly designed LNA can attenuate these undesired RF signals because most of the undesired RF frequencies fall outside the frequency range. A zero can be inserted in the LNA to remove the spurious frequency at 4.05 GHz.

The band selection at the 5.7-GHz band is depicted in Fig. 3(a). The solid-, dotted-, and dashed-line arrows represent the RF signal, IM_1 signal, and IM_2 signal, respectively. The RF signal, as well as the undesired IM_1 and IM_2 signals, are located at the positive spectrum, and down-converted by the $\mathrm{e}^{-j\omega_{\mathrm{LO1}}t}$ and $\mathrm{e}^{-j\omega_{\mathrm{LO2}}t}$ LO signals, respectively. As discussed above, the Weaver–Hartley architecture can reject both the first and secondary image signals. On the other hand, when the desired signals are around 2.4 GHz, the signals located at the negative spectrum are down-converted by the $\mathrm{e}^{j\omega_{\mathrm{LO1}}t}$ and $\mathrm{e}^{j\omega_{\mathrm{LO2}}t}$ LO signals, as shown in Fig. 3(b).

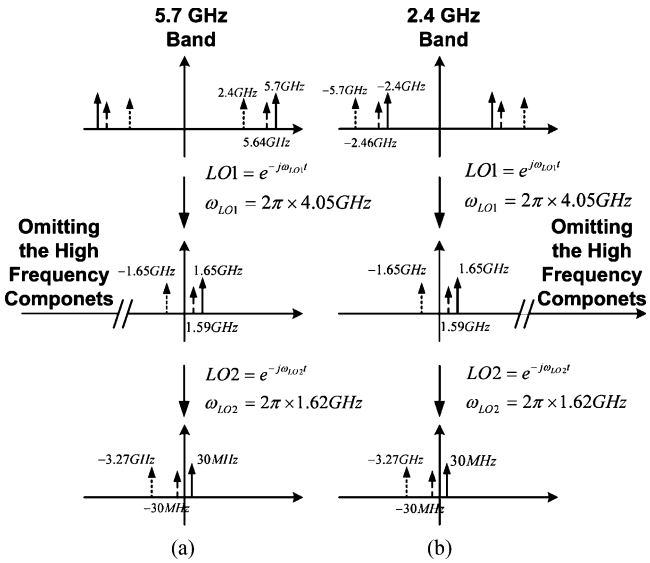

Fig. 3. All the high-frequency harmonics are neglected. (a) Frequency shifting by the negative LO_1 and negative LO_2 complex signals when the RF frequency is around 5.7-GHz band. (b) Frequency shifting by the positive LO_1 and negative LO_2 complex signals when the RF frequency is around 2.4-GHz band.

In the Weaver–Hartley system shown in Fig. 1, the band selection is achieved by intentionally changing the sequence of the complex LO_1 signals. The positive LO_1 sequence corresponds to $\mathrm{e}^{j\omega_{\mathrm{LO1}}t}$, while the negative LO_1 sequence corresponds to $\mathrm{e}^{-j\omega_{\mathrm{LO1}}t}$. The sequence of the complex LO_1 signal can be alternated using MOS switches. The MOS switching circuits are discussed in Section III.

III. Circuit Design

The block diagram of the demonstrated Weaver–Hartley down-converter is shown in Fig. 4. The first- and second-stage complex mixers contain two and four Gilbert multipliers, respectively. The 4.05-GHz LO_1 signal is fed externally and the 1.62-GHz LO_2 signal is generated from the LO_1 signal using the divide-by-five circuit and the frequency doubler. The quadrature generators shown in Fig. 4 are two-section polyphase filters to generate differential-quadrature signals from differential signals. A four-section polyphase filter and an IF buffer amplifier are located at the end of the down-converter. Each sub-circuit is discussed below.

A. Gilbert Mixers

The mixers in the first and second stages are Gilbert mixers, as shown in Fig. 5. The Gilbert active mixer has advantages in terms of higher conversion gain, smaller LO pumping power, and better port-to-port isolation when compared to passive mixers. A micromixer, as shown in Fig. 5(a), is adopted in the first-stage mixer for its broadband matching property and is suitable for the dual-band application [18], [25]. The second-stage mixer is a conventional Gilbert mixer, as shown in Fig. 5(b), employing a differential pair as the input stage. Source degenerated resistors are employed to increase the $\mathrm{IP}_{1\,\mathrm{dB}}$ of the second-stage Gilbert mixer. The high input impedance of the second-stage mixer also maintains the voltage gain of the preceding stage.

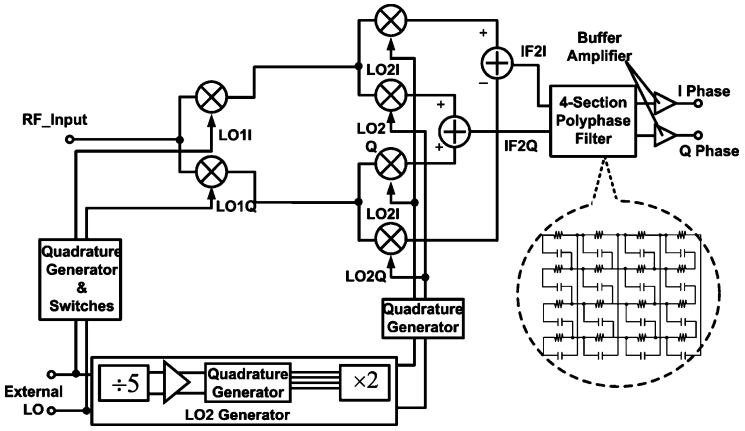

Fig. 4. Block diagram of the demonstrated Weaver–Hartley double-quadrature down-converter.

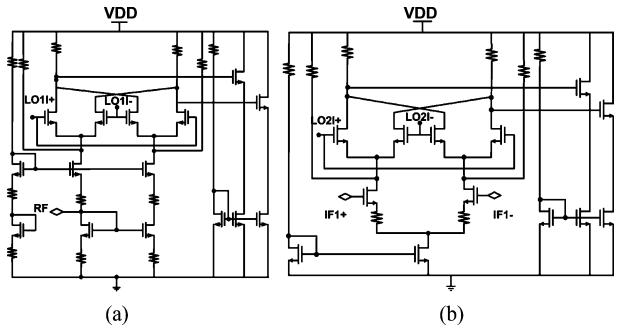

Fig. 5. Schematic of the Gilbert mixers used for the: (a) first- and (b) second-stage mixers.

The IF frequency of the first-stage mixer is around 1.65 GHz; therefore, the IF_1 bandwidth of the first-stage mixer is designed to be wide at the cost of gain. The source degeneration resistance in the second-stage mixer is relatively large in order to accommodate the wide IF_1 bandwidth and to achieve a good input dynamic range.

Moreover, the addition and subtraction for the complex mixing can be achieved by the current mode operation [18]. Connecting the output currents of the mixers in the in-phase way performs the function of addition, while the subtraction can be accomplished by connecting the output currents of the mixers in the antiphase way.

B. LO Frequency Generator

The image rejection depends on the magnitude and phase accuracies of LO and RF signals [9], [14], [15], [18]. The imperfect LO and RF signals are inevitable in the circuit fabrication, and thus, the image-rejection ratio degrades. Many methods such as off-chip or electronic tuning have been developed to increase the image-rejection performance [14], [15]. The coherence between the LO_1 and LO_2 signals improves the image rejection [18].

In order to achieve coherent LO signals, an accurate LO generator consisting of a 50% duty cycle divide-by-five circuit and a truly balanced frequency doubler [26]–[28] is employed to generate coherent signals with less phase errors. As a result, the frequency of the LO_1 signal is 2.5 times that of the LO_2 signal, and thus, only one VCO is needed.

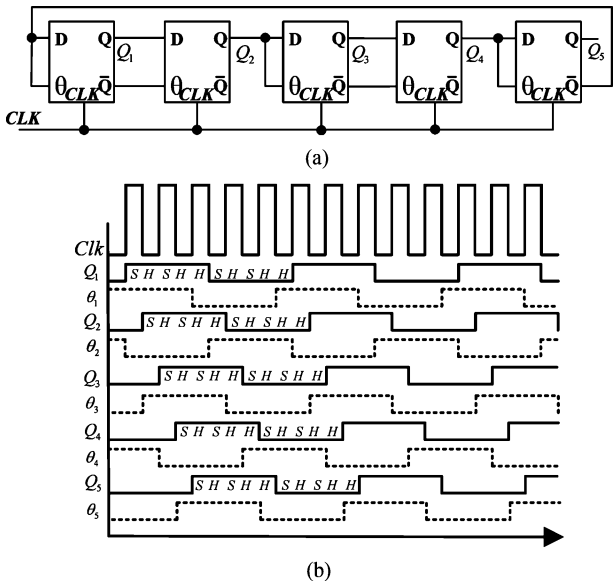

Fig. 6. (a) Block diagram of the 50% duty-cycle divide-by-five circuit. (b) Timing diagram.

As shown in Fig. 4, the LO generator consists of a divide-by-five circuit, buffer amplifier, quadrature generator, and frequency doubler. The block diagram of a 50% duty cycle divide-by-five circuit and its associated timing diagram are shown in Fig. 6(a) and (b), respectively. Non-50% duty cycle signals preceding a polyphase filter (quadrature generator) generate high-order harmonics and lead to large phase error [29], especially when the following circuit is a hard-switched Gilbert mixer (second-stage mixer). Therefore, the 50% duty cycle is critical for the Weaver–Hartley image-rejection system. The divide-by-five circuit consists of five current switchable source-coupled logic D flip-flops [29], [30] and employs the sample–hold–sample–hold–hold (SHSHH) scheme to achieve the 50% duty cycle. The schematic of the current switchable source coupled logic D flip-flop [29] is shown in Fig. 7. Two extra differential pairs with control inputs θ and $\bar{\theta}$ are inserted between the sample-and-hold stage and the clock stage of the traditional D flip-flop to commutate the clock current signal and switch the triggering edge of the clock for sample-and-hold. The input data is sampled when clock and θ are the same; on the

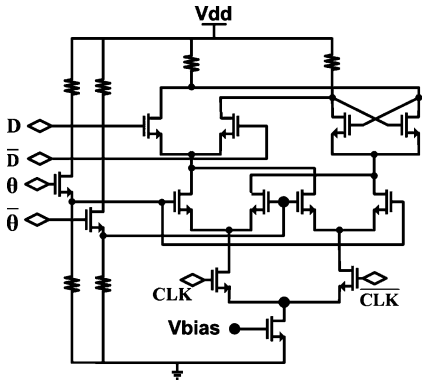

Fig. 7. Schematic of the current switchable source-coupled logic D flip-flop.

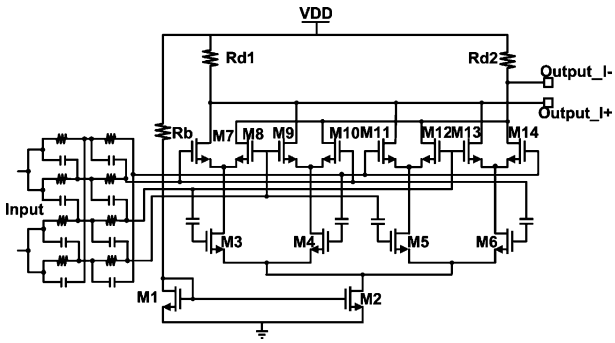

Fig. 8. Truly balanced multiplier and its input quadrature generator.

other hand, the data is held when they are opposite. Therefore, this current switchable D flip-flop can be triggered at both the positive and negative edges. A conventional Gilbert multiplier has a time delay between the signal through the bottom differential pair and the signal through the top differential pair, and thus, gives rise to asymmetrical output waveforms. To remedy this problem, a fully symmetrical multiplier circuit with equal delay paths between two input signals is adopted in this work. Fig. 8 shows a truly balanced frequency doubling multiplier consisting of two conventional Gilbert multipliers. The in- and quadrature-phase input signals connect to the top and bottom stages of one multiplier, respectively. On the other hand, the input signals of the other multiplier are connected in the opposite way. Therefore, one multiplying path contains a phase lead and the other path contains a phase lag. By summing the outputs of the two constituent multipliers, the phase delay is cancelled in the combined signals [27], [29]. The two-section polyphase filter in Fig. 8 generates quadrature signals needed by the truly balanced frequency doubler.

C. LO Switching Circuit

The 2.4/5.7-GHz band selections are achieved by changing the polarity of the LO_1 signals. Fig. 9 shows the band-selection switching circuits. When S1 is low and S2 is high, the 5.7-GHz band is selected. The LO_1 signals are in the clockwise sequence of $I+$, $Q-$, $I-$, and $Q+$, and can be represented by $\mathrm{e}^{-j\omega_{\mathrm{LO1}}t}$. On the other hand, the 2.4-GHz band is chosen when S1 is high and S2 is low. The LO_1 signals are in the counterclockwise sequence of $I+$, $Q+$, $I-$, and $Q-$, and thus, can be represented by

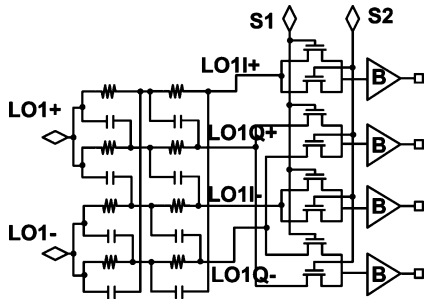

Fig. 9. LO_1 signal polarization switching circuit used to perform the band selection.

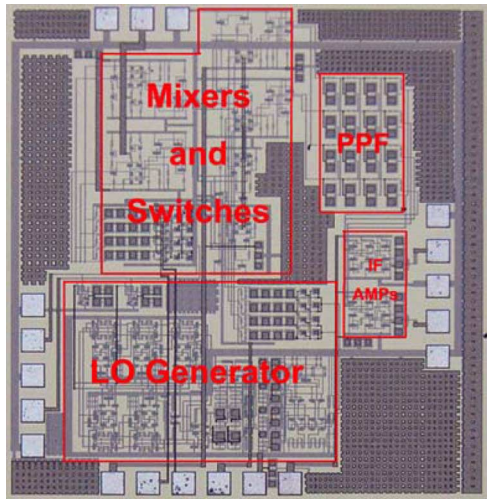

Fig. 10. Die photograph of the Weaver–Hartley dual-band low-IF down-converter.

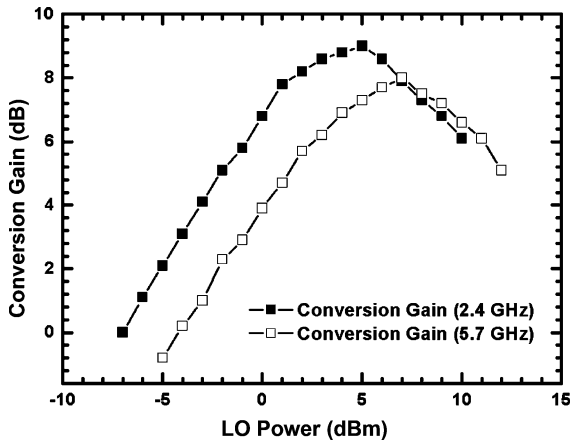

Fig. 11. Conversion gain as a function of LO power of the demonstrated Weaver–Hartley dual-band low-IF down-converter.

$\mathrm{e}^{j\omega_{\mathrm{LO1}}t}$. Buffer B is a common-drain-configured output buffer to drive the LO port of the mixer.

D. Polyphase Filter and IF Amplifier

The secondary image rejection of the Weaver–Hartley system relies on the polyphase filter. In order to obtain a 45-dB image-rejection ratio and a 12–48-MHz bandwidth, a four-section polyphase filter is incorporated at the end of the down-converter, as shown in Fig. 4. The buffer amplifiers

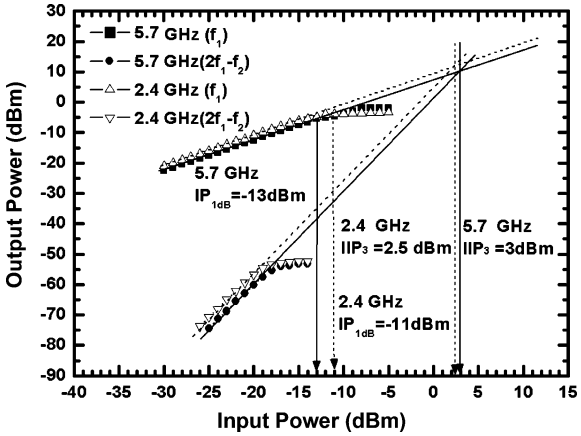

Fig. 12. Power performances of the demonstrated Weaver–Hartley dual-band low-IF down-converter.

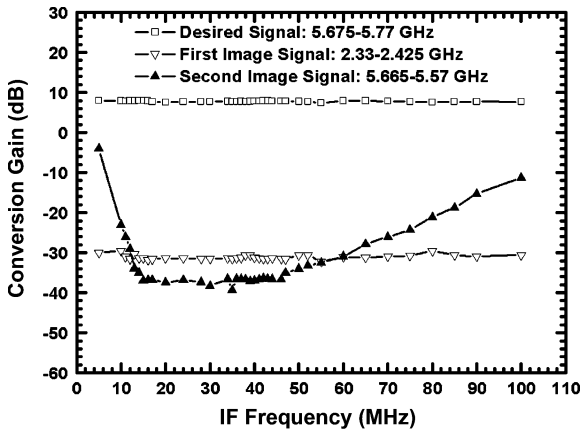

(a)

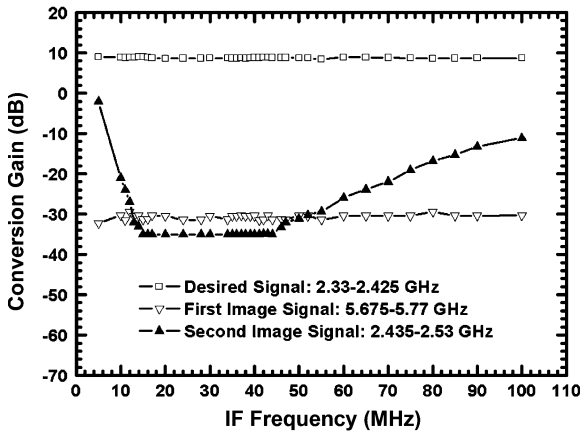

(b)

Fig. 13. Conversion gain as a function of RF and image frequencies of the demonstrated Weaver–Hartley dual-band low-IF down-converter. IF frequencies are employed to represent the RF and image frequencies by properly folding the RF and image frequencies into the IF axis (a) RF near 5.7 GHz. (b) RF near 2.4 GHz.

following the polyphase filter are employed mainly to drive the 50-Ω spectrum analyzer for the on-wafer measurement.

IV. Measurement Results

A die photograph of the Weaver–Hartley down-converter is shown in Fig. 10, and the die size is 2×2 mm^2. The RF, IF, LO

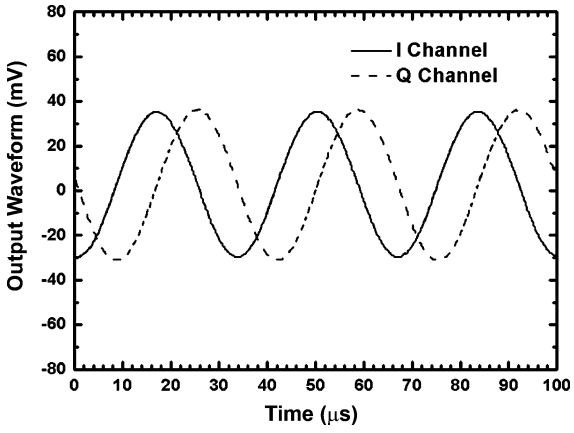

Fig. 14. Measured I/Q waveform (with 90.55° phase difference) of the demonstrated Weaver–Hartley dual-band low-IF down-converter.

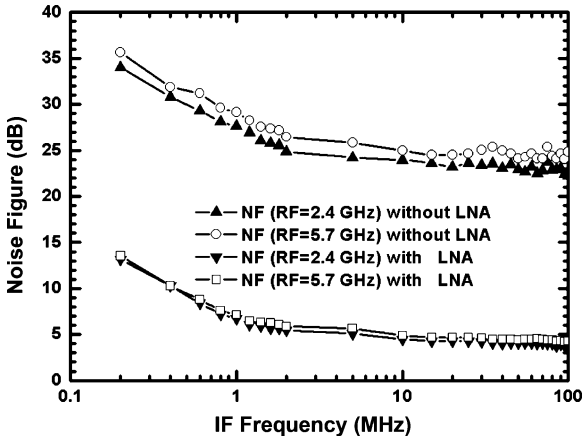

Fig. 15. Measured NF of the Weaver–Hartley dual-band low-IF down-converter with/without the external LNA.

ground–signal–ground–signal–ground (GSGSG), and six-pin dc pads are located at the top, right, left, and bottom of the die in sequence. The layout is very compact and many bypass capacitors are used to verify the effectiveness of both the dc supply and the area occupied by the dummy metal cells. The supply voltage is 1.8 V and the power consumption of the main mixer cores are only 25 mW while the LO generator consume 54 mW. However, the common-drain buffers following the active mixers in Fig. 5 totally consumes 20 mW and this dc power consumption is over designed. The buffer current can be reduced drastically because both IF_1 and IF_2 frequencies are low. Besides, the IF buffer amplifiers, consuming 13 mW for each in-phase/quadrature (I/Q) output path, are employed mainly to drive the 50-Ω spectrum analyzer for the on-wafer measurement; however, it can be eliminated from our receiver architecture for a practical application due to the high input impedance of the following circuits. Fig. 11 shows the conversion gain as a function of LO power for the 2.4-GHz band. The conversion gain reaches 9 dB when the LO power is larger than 5 dBm. On the other hand, the peak conversion is 8 dB when the RF frequency is 5.7 GHz and the LO power is larger than 7 dBm.

When the RF frequency is 5.7 GHz, the demonstrated down-converter has an $\mathrm{IP}_{1\,\mathrm{dB}}$ of -13 dBm and IIP_3 of 3 dBm, as

TABLE I
COMPARISON OF IMAGE-REJECTION RATIO

Reference	Architecture	Frequency(GHz)	IRR_1	IRR_2	Noise Figure(dB)	Power Consumption (mW)	Technology
[14]	Weaver	1.9	45	N.A. [b]	14	198 [e]	0.6-μm CMOS
[10]	Weaver-Hartley	2.4	35	60 [c]	7.2	115.5	0.6-μm CMOS
[16]	Weaver Dual-band	0.9/1.8	40/36	N.A. [b]	4.7/4.9	75	0.6-μm CMOS
[17]	Weaver-Hartley	0.9	55 [a]	35	5	70	0.35-μm CMOS
This Work	Weaver-Hartley Dual-band	2.4/5.7	40/40	44/46	23/25 (4.2/4.65) [d]	126 [f] (mixer cores: 25)	0.18-μm CMOS

[a]performance with a preceding narrow band LNA.
[b]IF_2=0.
[c]5-section polyphase filter and passive IF mixers.
[d]Noise figure measured with an wideband external LNA.
[e]Power consumption including ADC and baseband filter.
[f]Total power consumption includes the main mixer core (25 mW), LO generator (54 mW) , mixer buffers (20 mW) and extra IF output buffers (26 mW) facilitating the on-wafer 50-Ω measurement.

shown in Fig. 12. When the RF frequency is 2.4 GHz, $\mathrm{IP}_{1\ \mathrm{dB}}$ and IIP_3 are -11 dBm and 2.5 dBm, respectively.

Fig. 13 shows the conversion gain as a function of RF frequencies. LO_1 frequency is fixed at 4.05 GHz, and thus, LO_2 is equal to 1.62 GHz. The RF frequency is swept to obtain the gain difference between the desired signal and images. The resulting IF frequencies are employed to represent the RF and image frequencies by properly folding the RF and image frequencies into the IF axis.

When the desired RF signal is around 5.7 GHz, the frequencies of the desired IF signal, the IF signals caused by the first image signal, and the second image signal can be calculated by

$$\mathrm{IF}_{\mathrm{desired}} = \mathrm{RF} - \mathrm{LO}_1 - \mathrm{LO}_2 \tag{3a}$$
$$\mathrm{IF}_{\mathrm{IM1}} = \mathrm{LO}_1 - \mathrm{IM}_1 - \mathrm{LO}_2 \tag{3b}$$
$$\mathrm{IF}_{\mathrm{IM2}} = \mathrm{LO}_1 + \mathrm{LO}_2 - \mathrm{IM}_2. \tag{3c}$$

On the other hand, when the desired RF signal is around 2.4 GHz, the frequencies of the desired IF signal, the IF signal caused by the first image signal, and the second image signal can be calculated by

$$\mathrm{IF}_{\mathrm{desired}} = \mathrm{LO}_1 - \mathrm{RF} - \mathrm{LO}_2 \tag{4a}$$
$$\mathrm{IF}_{\mathrm{IM1}} = \mathrm{IM}_1 - \mathrm{LO}_1 - \mathrm{LO}_2 \tag{4b}$$
$$\mathrm{IF}_{\mathrm{IM2}} = \mathrm{IM}_2 - \mathrm{LO}_1 + \mathrm{LO}_2. \tag{4c}$$

As shown in Fig. 13(a), the gain of the desired signal is 8 dB when the RF signal frequency is around 5.7 GHz. On the other hand, the first image signal near 2.4 GHz has a conversion loss of 32 dB, and the conversion loss of the secondary image signal (5.64 GHz) is 38 dB. Similarly, the gain is 9 dB when the desired RF signal frequency is around 2.4 GHz, as shown in Fig. 13(b). The first image signal (near 5.7 GHz) and secondary image signal (near 2.46 GHz) have a conversion loss of 31 and 35 dB, respectively.

In other words, when the RF frequency is 5.7 GHz (2.4 GHz), the image-rejection ratios of the first and secondary image signals are about 40 dB (40 dB) and 46 dB (44 dB), respectively. The frequency response of the secondary image signal is a bandstop shape because of the complex filtering behavior of the polyphase filter. The IF bandwidth of the measured image-rejection ratio of the secondary image signal starts from 12 to 48 MHz. On the other hand, the image-rejection ratio of the first image signal has a flat frequency response because the image-rejection mechanism of the Weaver system comes from dual LO frequency shifting, as discussed in Fig. 2.

Fig. 14 shows the waveforms of I/Q output ports. The measured result indicates that the output signals are quite balanced. The in- and quadrature-phase waveforms also demonstrate that the circuit is highly balanced, including the signal phase and signal magnitude.

The measured RF-to-IF, LO-to-RF, and LO-to-IF isolations are better than 60, 64, and 62 dB, respectively. The measured NF of the down-converter is shown in Fig. 15. When the RF frequencies are 2.4 and 5.7 GHz, the measured NFs are better than 23 dB and 25 dB within the 12-MHz to 48-MHz IF bandwidth. A CMOS device suffers from a serious flicker noise problem. It is obvious that the flicker noise corner frequency in Fig. 15 is around 2 MHz for this architecture. Thus, the serious flicker noise problem is avoided in our demonstrated low-IF architecture by arranging the IF frequencies to be from 12 to 48 MHz [17].

The micromixer with the wideband 50-Ω matching at the input stage facilitates the RF measurement and is employed in this paper to demonstrate the proposed dual-band image-rejection receiver architecture without using a preceding LNA (or filter). However, this resistive matching topology degrades the noise performance. A high-gain LNA is needed to improve the noise performance at the cost of overall system linearity. Thanks to the wideband matching, the demonstrated down-converter is convenient for connecting an external LNA to measure the overall receiver NF. Two commercial broadband LNAs (LNA_1 : gain $= 11$ dB and $\mathrm{NF} = 2$ dB; LNA_2 : gain $= 20$ dB and $\mathrm{NF} = 5$ dB) and a 9-dB attenuator are employed to form an *ad hoc* LNA. Thus, the *ad hoc* broadband LNA has a 22-dB gain with 2.65-dB NF over 1–8 GHz. After cascading the LNA, the measured NF of the receiver is highly suppressed to 4.2 dB at $\mathrm{RF} = 2.4$ GHz and 4.65 dB at $\mathrm{RF} = 5.7$ GHz, respectively, as shown in Fig. 15. After cascading the LNA, the measured $\mathrm{IP}_{1\ \mathrm{dB}}$ is $-33.2/-34.5$ dBm for each 2.4/5.7-GHz band, and is still acceptable for the high-gain mode in wireless local area network (WLAN) application. If better noise and linearity are required in the receiver, a conventional Gilbert mixer with a band-switchable input transconductance stage for dual-band operation can be employed [22]. An inductive source degeneration technique widely used in the LNA can be employed in

the transconductance stage of a Gilbert mixer to bring the noise circle and gain circle closer [31].

The state-of-the-art image-rejection ratio results for the various architectures are summarized in Table I.

V. Conclusion

A new image-rejection low-IF topology combining the Weaver and Hartley systems has been demonstrated via complex signal analysis in this paper, and a dual-band down-converter has been implemented using the proposed topology. In this study, the quadrature LO signals has been employed in the RF stage mixers and the band selection has been achieved by changing the polarity of the complex LO_1 signal. The image-rejection ratio was further improved by making two LO signals coherent with the proposed new divider. As a result, the low-IF dual-band down-converter only requires one on-chip VCO, and the RF mixers are reused for both 2.4/5.7-GHz bands. Thus, complexity is greatly reduced. Furthermore, the diagrammatic complex mixing explanation developed in this paper gives the RF designers a clear illustration to design the image-rejection system.

Acknowledgment

The authors would like to thank the National Chip Implementation Center (CIC), Hsinchu, Taiwan, for technical support.

References

[1] A. A. Abidi, "Direct-conversion radio transceivers for digital communications," *IEEE J. Solid-State Circuits*, vol. 30, no. 12, pp. 1399–1410, Dec. 1995.

[2] H. Darabi and A. A. Abidi, "Noise in RF-CMOS mixers: A simple physical model," *IEEE J. Solid-State Circuits*, vol. 35, no. 1, pp. 15–25, Jan. 2000.

[3] L. Sheng, J. C. Jensen, and L. E. Larson, "A wide-bandwidth Si/SiGe HBT direct conversion sub-harmonic mixer/downconverter," *IEEE J. Solid-State Circuits*, vol. 35, no. 9, pp. 1329–1337, Sep. 2000.

[4] K.-J. Koh, M.-Y. Park, C.-S. Kim, and H.-K. Yu, "Subharmonically pumped CMOS frequency conversion (up and down) circuits for 2-GHz WCDMA direct-conversion transceiver," *IEEE J. Solid-State Circuits*, vol. 39, no. 6, pp. 871–884, Jun. 2004.

[5] H. Darabi and J. Chiu, "A noise cancellation technique in active RF-CMOS mixers," *IEEE J. Solid-State Circuits*, vol. 40, no. 12, pp. 2628–2632, Dec. 2005.

[6] J. Yoon, H. Kim, C. Park, J. Yang, H. Song, S. Lee, and B. Kim, "A new RF CMOS Gilbert mixer with improved noise figure and linearity," *IEEE Trans. Microw. Theory Tech.*, vol. 56, no. 3, pp. 626–631, Mar. 2008.

[7] S. Zhou and M. C. F Chang, "A CMOS passive mixer with low flicker noise for low-power direct-conversion receiver," *IEEE J. Solid-State Circuits*, vol. 40, no. 5, pp. 1084–1093, May 2005.

[8] R. Hartley, "Modulation system," U.S. Patent 1 666 206, Apr. 17, 1928.

[9] F. Behbahani, Y. Kishigami, J. Leete, and A. A. Abidi, "CMOS mixers and polyphase filters for large image rejection," *IEEE J. Solid-State Circuits*, vol. 36, no. 6, pp. 873–887, Jun. 2001.

[10] F. Behbahani, J. C. Leete, Y. Kishigami, A. Roithmeier, K. Hoshino, and A. A. Abidi, "A 2.4-GHz low-IF receiver for wideband WLAN in 0.6-μm CMOS-architecture and front-end," *IEEE J. Solid-State Circuits*, vol. 35, no. 12, pp. 1908–2000, Dec. 2000.

[11] J. Crols and M. Steyaert, "A single-chip 900-MHz CMOS receiver front-end with a high-performance low-IF topology," *IEEE J. Solid-State Circuits*, vol. 30, no. 12, pp. 1483–1492, Dec. 1995.

[12] S. J. Fang, A. Bellaouar, S. T. Lee, and D. J. Allstot, "An image-rejection down-converter for low-IF receivers," *IEEE Trans. Microw. Theory Tech.*, vol. 53, no. 2, pp. 478–487, Feb. 2005.

[13] D. Weaver, "A third method of generation and detection of single-sideband signals," *Proc. IRE*, vol. 44, no. 12, pp. 1703–1705, Dec. 1956.

[14] J. C. Rudell, J.-J. Ou, T. B. Cho, G. Chien, F. Brianti, J. A. Weldon, and P. R. Gray, "A 1.9-GHz wide-band if double conversion CMOS integrated receiver for cordless telephone applications," *IEEE J. Solid-State Circuits*, vol. 32, no. 12, pp. 2071–1088, Dec. 1997.

[15] M. A. I. Elmala and S. H. K. Embabi, "Calibration of phase and gain mismatches in Weaver image-reject receiver," *IEEE J. Solid-State Circuits*, vol. 39, no. 2, pp. 283–289, Feb. 1998.

[16] S. Wu and B. Razavi, "A 900-MHz/1.8-GHz CMOS receiver for dual-band applications," *IEEE J. Solid-State Circuits*, vol. 33, no. 12, pp. 2178–2185, Dec. 1998.

[17] S. Tadjpour, E. Cijvat, E. Hegazi, and A. A. Abidi, "A 900-MHz dual-conversion IF GSM receiver in 0.35-μm CMOS," *IEEE J. Solid-State Circuits*, vol. 36, no. 12, pp. 1992–2002, Dec. 2001.

[18] T. H. Wu and C. C. Meng, "5.2/5.7 GHz 48 dB image rejection GaInP/GaAs HBT Weaver down-converter using LO frequency quadrupler," *IEEE J. Solid-State Circuits*, vol. 41, no. 11, pp. 2468–2480, Nov. 2006.

[19] O. Charlon, M. Locher, H. A. Visser, D. Duperray, J. Chen, M. Judson, A. L. Landesman, C. Hritz, U. Kohlschuetter, Y. Zhang, C. Ramesh, A. Daanen, M. Gao, S. Haas, V. Maheshwari, A. Bury, G. Nitsche, A. Wrzyszcz, W. R. White, H. Bonakdar, R. E. Waffaoui, and M. Bracey, "A low-power high-performance SiGe BICMOS 802.11 a/b/g transceiver IC for cellular and bluetooth co-existence applications," *IEEE J. Solid-State Circuits*, vol. 41, no. 7, pp. 1503–1512, Jul. 2006.

[20] A. Behzad, K. A. Carter, H.-M. Chien, S. Wu, M.-A. Pan, C. P. Lee, Q. Li, J. C. Leete, S. Au, M. S. Kappes, Z. Zhou, D. Ojo, L. Zhang, A. Zolfaghari, J. Castanada, H. Darabi, B. Yeung, A. Rofougaran, M. Rofougaran, J. Trachewsky, T. Moorti, R. Gaikwad, A. Bagchi, J. S. Hammerschmidt, J. Pattin, J. J. Rael, and B. Marholev, "A fully integrated MIMO multiband direct conversion CMOS transceiver for WLAN applications (802.11n)," *IEEE J. Solid-State Circuits*, vol. 42, no. 12, pp. 2795–2808, Dec. 2007.

[21] M. Zargari, M. Terrovitis, S. H. M. Jen, B. J. Kaczynski, M. Lee, M. P. Mack, S. S. Mehta, S. Mendis, K. Onodera, H. Samavati, W. W. Si, K. Singh, A. Tabatabaei, D. Weber, D. K. Su, and B. A. Wooley, "A single-chip dual-band tri-mode CMOS transceiver for IEEE 802.11a/b/g wireless LAN," *IEEE J. Solid-State Circuits*, vol. 39, no. 12, pp. 2239–2249, Dec. 2004.

[22] R. Ahola, A. Aktas, J. Wilson, K. R. Rao, F. Jonsson, I. Hyyryläinen, A. Brolin, T. Hakala, A. Friman, T. Mäkiniemi, J. Hanze, M. Sandén, D. Wallner, Y. Guo, T. Lagerstam, L. Noguer, T. Knuuttila, P. Olofsson, and M. Ismail, "A single-chip CMOS transceiver for 802.11a/b/g wireless LANs," *IEEE J. Solid-State Circuits*, vol. 39, no. 12, pp. 2250–2258, Dec. 2004.

[23] C.-Y. Chou and C.-Y. Wu, "The design of wideband and low-power CMOS active polyphase filter and its application in RF double-quadrature receivers," *IEEE Trans. Circuits Syst., Reg. Papers*, vol. 52, no. 5, pp. 825–833, May 2005.

[24] H. Hashemi and A. Hajimiri, "Concurrent multiband low-noise amplifiers—Theory, design, and applications," *IEEE Trans. Microw. Theory Tech.*, vol. 50, no. 1, pp. 288–301, Jan. 2002.

[25] B. Gilbert, "The MICROMIXER: A highly linear variant of the Gilbert mixer using a bisymmetric class-AB input stage," *IEEE J. Solid-State Circuits*, vol. 32, no. 9, pp. 1412–1423, Sep. 1997.

[26] A. W. Buchwald and K. W. Martin, "High-speed voltage-controlled oscillator with quadrature outputs," *Electron. Lett.*, vol. 27, no. 4, pp. 309–310, Feb. 1991.

[27] A. W. Buchwald, K. W. Martin, A. K. Oki, and K. W. Kobayashi, "A 6-GHz integrated phase-locked loop using AlGaAs/GaAs heterojunction bipolar transistors," *IEEE J. Solid-State Circuits*, vol. 27, no. 12, pp. 1752–1762, Dec. 1992.

[28] R. Magoon, A. Molnar, J. Zachan, G. Hatcher, and W. Rhee, "A single-chip quad-band (850/900/1800/1900 MHz) direct conversion GSM/GPRS RF transceiver with integrated VCOs and franctional-N synthesizer," *IEEE J. Solid-State Circuits*, vol. 37, no. 12, pp. 1710–1720, Dec. 2002.

[29] R. Magoon and A. Molnar, "RF local oscillator path for GSM direct conversion transceiver with true 50% duty cycle divide by three and active third harmonic cancellation," in *RFIC Symp. Dig.*, Seattle, WA, 2002, pp. 23–26.

[30] S. C. Tseng, C. Meng, and W. Y. Chen, "True 50% duty-cycle SSH and SHH SiGe BiCMOS divide-by-3 prescalers," *IEICE Trans. Electron.*, vol. E89-C, no. 6, pp. 725–731, 2006.

[31] T.-K. Nguyen, C.-H. Kim, G.-J. Ihm, M.-S. Yang, and S.-G. Lee, "CMOS low-noise amplifier design optimization techniques," *IEEE Trans. Microw. Theory Tech.*, vol. 52, no. 5, pp. 1433–1442, May 2004.

Chin-Chun Meng (M'02) received the B.S. degree in electrical engineering from National Taiwan University, Taipei, Taiwan, in 1985, and the Ph.D. degree in electrical engineering from the University of California at Los Angeles (UCLA), in 1992.

He is currently a Full Professor with the Department of Communication Engineering, National Chiao Tung University, Hsinchu, Taiwan. His current research interests are in the areas of RF integrated circuits (RFICs), microwaves, and millimeter-wave integrated circuits.

Tzung-Han Wu (S'06–M'08) was born in Taipei, Taiwan, in 1979. He received the B.S. and M.S. degrees in electrical engineering from National Chung Hsing University, Taichung, Taiwan, in 2001 and 2003, respectively, and the Ph.D. degree in communication engineering from National Chiao-Tung University, Hsinchu, Taiwan, in 2007. His M.S. degree concerned GaInP/GaAs HBT, SiGe HBT, and CMOS wideband amplifiers and mixers.

He is currently with MediaTek, Hsinchu, Taiwan. His current research interests are RFICs and analog integrated circuits (ICs).

Dr. Wu is a member of Phi Tau Phi.

Jin-Siang Syu was born in Taoyuan, Taiwan, in 1984. He received the B.S. degree in communication engineering from National Chiao Tung University, Hsinchu, Taiwan, in 2006, and is currently working toward the Ph.D. degree in communication engineering at National Chiao Tung University.

His current research interests are in the areas of RFICs.

Mr. Syu is a member of Phi Tau Phi.

Sheng-Wen Yu was born in I-Lan, Taiwan, in 1982. He received the B.S. degree in electrical engineering from National Chung Cheng University, Chia-Yi, Taiwan, in 2005, and is currently working toward the Master degree in communication engineering at National Chiao Tung University, Hsinchu, Taiwan.

His current research interests are in the areas of RFICs.

Kuan-Chang Tsung was born in Nantou, Taiwan, in 1983. He received the B.S. degree in electrical engineering from National Cheng Kung University, Tainan, Taiwan, in 2005, and is currently working toward the M.S. degree in communication engineering from National Chiao Tung University, Hsinchu, Taiwan.

Ya-Hui Teng was born in Pingtung, Taiwan, in 1983. She received the B.S. degree in communication engineering from National Chiao Tung University, Hsinchu, Taiwan, in 200, and is currently working toward the M.S. degree in communication engineering at National Chiao Tung University.

Her research interests include RFICs and analog ICs.